

1 **Assessment of riverbed evolution in the Vam Nao River under the influence of sand mining**
2 **using a numerical model**

3 Nguyen Dam Quoc Huy^{a,b}, Tran Thi Kim^{a,b*}

4 ^aUniversity of Science, 227 Nguyen Van Cu, Cho Quan Ward, Ho Chi Minh City 700000, Vietnam, Email:
5 ndqhuy@imhoen.com.vn, ttkim@hcmus.edu.vn;

6 ^bVietnam National University, Dong Hoa Ward, Ho Chi Minh City, Vietnam

7 *Corresponding author. Email: ttkim@hcmus.edu.vn (0000-0001-5748-3371)

8 **ABSTRACT**

9 Riverbed sand mining is a major anthropogenic driver of sediment imbalance and riverbank erosion in the Mekong
10 Delta. This study investigates its morphological impacts using the hydrodynamic–morphological model HYDIST,
11 coupled with a sand mining source function (S_{sm}), to directly simulate unsustainable sand mining. The model is applied
12 to the Vam Nao River, a confluence connecting the Tien and Hau rivers. Unlike conventional approaches that assume
13 static mining pits, sand mining is represented here as a dynamic process by incorporating the source function directly
14 into the bed evolution equation, allowing a more realistic description of mining–morphology interactions.

15 Simulation results show that sand mining markedly intensifies riverbed erosion and disrupts the natural erosion–
16 deposition balance. In the Vam Nao River reach (Zone 1), the proportion of deposition declines from 27.1% to 12.9%,
17 while erosion increases to 87.1% of total morphological change, indicating a transition toward an erosion-dominated
18 regime. In the Hau River reach (Zone 2), which is naturally depositional with deposition accounting for up to 83.77%
19 under non-mining conditions, sand mining completely reverses the morphological pattern. The total erosion volume
20 becomes 8.4 times greater than that in the non-mining scenario. At the Vam Nao–Hau River confluence (Zone 3),
21 deposition volume decreases by 30.2%, and erosion represents 69.56% of total morphological change, highlighting a
22 strong downstream propagation of mining impacts. The results demonstrate that sand mining substantially enhances
23 morphological instability, particularly in river confluence zones, and that these zones play a critical role in amplifying
24 the effects of upstream sand mining.

25 **Keywords:** Sand mining; Riverbed morphology; Hungry water; Sediment budget; Mekong Delta

26 (1) This is a non-peer reviewed preprint on EarthArXiv, and (2) the manuscript is also under review at Hydrology
27 Research.

28 HIGHLIGHTS

- 29 • Sand mining shifts the river from balanced conditions to strong erosion, rapidly deepening the riverbed.
- 30 • Areas that once trapped sediment begin eroding, increasing risks of bank collapse and channel instability.
- 31 • Impacts spread downstream, showing that mining effects extend far beyond the extraction sites.

32 1. INTRODUCTION

33 Sand mining is a dual nature activity, as it can both contribute to flow regulation and the restoration of natural riverbed
34 morphology ([KoeHNken et al. 2020](#); [Rentier and Cammeraat 2022](#)), while at the same time posing potential risks of
35 hydrodynamic alteration, erosion, groundwater level decline ([Farahani and Bayazidi 2018](#); [Hackney et al. 2020a](#);
36 [Rentier and Cammeraat 2022](#); [Sonak et al. 2006](#); [Padmalal and Maya 2014a](#)), resource scarcity, and saltwater intrusion
37 ([Loc et al. 2021](#); [Park et al. 2022](#)). Worldwide, numerous studies have pointed out the consequences of sand extraction
38 exceeding natural thresholds. In China, Luo and co-authors (2007) found that sand dredging in the Pearl River Delta
39 increased channel slope, caused bank instability, and enhanced saltwater intrusion, in addition to benefits such as flood
40 reduction and improved inland navigation ([Luo et al. 2007](#)). Similarly, Ashraf and co-authors (2011) warned that
41 extraction exceeding natural replenishment capacity at Bestari Jaya (Malaysia) led to downstream erosion, flow
42 alteration, and increased water turbidity ([Ashraf et al. 2011](#)). More recently, Rentier and co-authors (2022) synthesized
43 the multidimensional impacts of sand mining on the physical environment (river widening), biological aspects
44 (biodiversity decline), chemical components (water and soil pollution), and social dimensions (infrastructure damage
45 and labor risks) ([Rentier and Cammeraat 2022](#)).

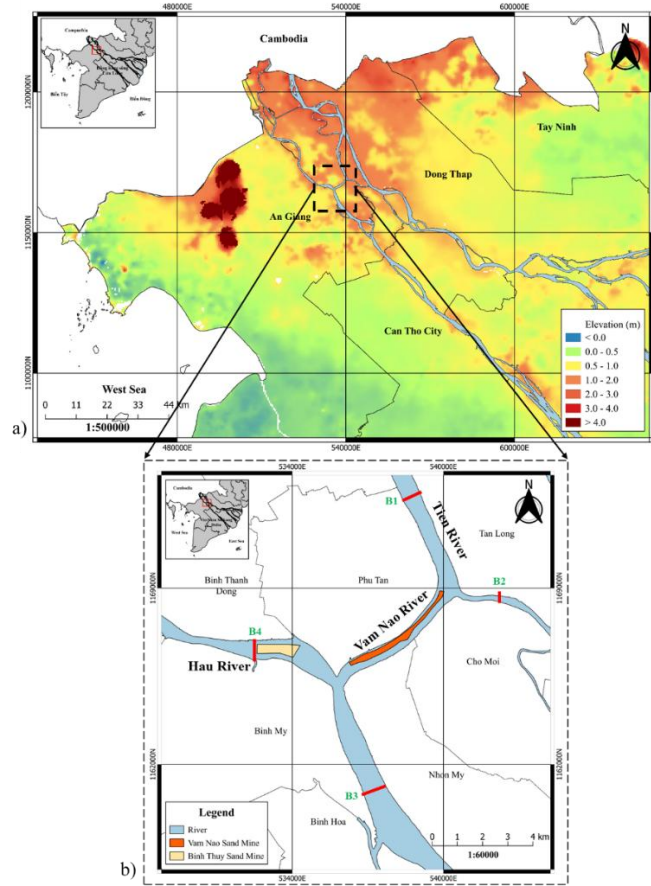
46 In the Mekong Delta, sand mining has become a critical issue due to increasing construction demand and
47 reduced sediment supply from the upstream Mekong River ([Jordan et al. 2019](#); [Kummu et al. 2008](#); [Miyazawa et al.
48 2008](#)). Unsustainable extraction has created localized scour pits and disrupted flow structures ([Anthony et al. 2015](#);
49 [Kim et al. 2020](#); [Brunier et al. 2014](#); [Barman et al. 2018](#)), especially when sediment replenishment is insufficient,
50 leading to uncontrolled expansion of erosion pits ([Kondolf 1997](#); [Barman et al. 2019](#); [Padmalal and Maya 2014b](#); [Kim
51 et al. 2020](#)). Bravard and co-authors (2013) estimated that approximately 50 million tons of sand per year are extracted
52 from the Mekong Delta, mainly in Cambodia and Vietnam ([Bravard et al. 2013](#)). The study by Gruel and co-authors
53 (2022) showed that during the period 2015–2020, the Tien River (upstream of My Thuan) accounted for 66% of the
54 total sand extraction volume in the region (167.17 million m³), while the Hau River accounted for only 17%.
55 Downstream of My Thuan, there are areas with lower extraction intensity, with an extracted volume of 42.19 million
56 m³, accounting for about 17% of the total reserves. Compared to the Tien River, the Hau River has a lower extraction
57 rate of 44.22 million m³, representing approximately 17% of the total extracted volume ([Gruel et al. 2022](#)). The direct
58 consequence is increased riverbank erosion, with more than 665 erosion sites recorded up to 2019, mainly concentrated
59 along the Tien River and the Hau River, with a total affected length exceeding 224 km ([Bay 2017 - 2021](#)).
60 Unsustainable sand mining combined with sediment reduction has rapidly lowered riverbed levels. Christopher R.
61 Hackney (2020) pointed out that sand mining activities along the Mekong River currently exceed allowable levels,
62 causing significant changes in river hydrodynamic and morphological processes ([Hackney et al. 2020b](#)). Nguyen
63 Nghia Hung and co-authors (2020) indicated that the rate of riverbed lowering in the Mekong Delta during the period
64 2008–2018 reached up to 15.3 cm per year, which is substantially higher than the rates of land subsidence (1–2.5 cm
65 per year) and sea level rise ([Hung et al. 2020](#)). This has altered tidal regimes, increased saltwater intrusion, and
66 threatened freshwater resources. Climate change further exacerbates this situation through seasonal flow alteration,
67 increased droughts, and intensified storms and floods ([Bay et al. 2023](#); [Dang and Pokhrel 2024](#); [Vu et al. 2024](#)). Sand
68 mining is one of the contributing factors to riverbed incision, accounting for approximately 2.9% (ranging from 2.6%
69 to 3.6%) of incision in the Tan Chau – My Thuan reach of the Tien River and Vam Kenh. Binh and co-authors (2020)
70 suggested that if sand mining activities across the entire Mekong Delta reach a volume of 7.75 million m³ per year,
71 as mentioned in ([Bravard et al. 2013](#)), they could contribute up to 14.8% of the total observed incision volume. It is
72 noteworthy that this percentage could be even higher, as sand mining operators often underreport extraction volumes
73 to reduce associated costs ([Bravard et al. 2013](#)). In addition, sand mining in the Mekong Delta is mainly carried out
74 using rudimentary tools such as shovels, involves illegal sand extraction, and the continued practice of excessive
75 mining activities, which together contribute to making the region increasingly difficult to manage ([Ng and Park 2021](#)).

76 Many studies have applied advanced technologies to predict and mitigate risks in the Mekong Delta. Binh and
77 co-authors (2022) simulated the formation of 16 scour holes on the Tien–Hau River system during 2014–2017 and
78 predicted the development of an additional 22 scour holes by 2026 if sediment supply continues to decline. This study
79 focused on identifying and tracking the dynamic evolution of scour holes within the river channel, reflecting their
80 migration and expansion over time. However, sand mining activities in this study were not simulated as a continuous
81 process in time, but were mainly considered indirectly through changes in riverbed morphology and reductions in
82 sediment supply ([Binh et al. 2022](#)). Kim and co-authors (2020) modeled the impacts of sand mining on morphological
83 changes and the expansion of scour holes along the Tien River reach flowing through Tan Chau town using the
84 HYDIST–GPUs model, which allows the assessment of time varying impacts of sand mining ([Kim et al. 2020](#)). More
85 recently, Thi Huong Vu and co-authors (2025) combined deep learning, satellite imagery, and the Delft3D-FLOW
86 model to assess the impacts of sand mining on riverbed morphology in the Mekong Delta. The impacts of sand mining
87 in this study were primarily represented in the model as erosion pits and static extraction zones, with no temporal
88 variability ([Vu et al. 2025](#)).

89 Overall, previous studies have demonstrated the link between sand mining, riverbed erosion, and environmental
90 degradation; however, most numerical models still rely on the assumption of mining pits with fixed shapes and
91 locations. This approach does not fully capture the dynamic nature of sand mining processes, in which dredging
92 activities occur continuously over time and directly interact with sediment transport processes and riverbed
93 morphological evolution ([Binh et al. 2022](#); [Gruel et al. 2022](#); [Rentier and Cammeraat 2022](#); [Kim et al. 2020](#)). Based
94 on these considerations, the present study applies the HYDIST model with the integration of a sand mining source
95 function, enabling the simulation of unsustainable sand mining as a dynamic component of the system, and thereby
96 allowing a quantitative assessment of riverbed morphological changes both within mining areas and in river reaches
97 affected by propagated impacts. The study area is the Vam Nao River reach, which plays a key role in conveying large
98 discharges, exhibits strong flow fields and high morphological variability, and is also a zone of concentrated large
99 scale sand mining activities. The application of the HYDIST model at this highly sensitive location enables the
100 assessment not only of local impacts of sand mining at mining sites, but also of propagated effects on the confluence
101 zone and adjacent river reaches, thereby clarifying the relationship between sand mining and channel instability at one
102 of the most important hydrodynamic nodes of the Mekong River system.

103 **2. STUDY AREA**

104 The Vam Nao River, an important watercourse within the Mekong River system, occupies a distinctive geographical
105 position in An Giang Province, Viet Nam. The river functions as a natural hydraulic link between the two main
106 branches, the Tien River and the Hau River, forming a unique hydrological structure within the Mekong Delta
107 ([Winemiller et al. 2016](#)). According to reports from the Department of Agriculture and Environment, during the 2019
108 flood season, high discharges combined with strong currents caused localized bank erosion in several areas of Cho
109 Moi and Nhon My communes ([An Giang Provincial Department of Natural Resources and Environment 2021](#)). For
110 this reason, the project “Dredging and river training of the Vam Nao River to mitigate bank erosion in My Hoi Dong
111 commune and Kien An commune, Cho Moi district, An Giang Province”, located along the river reach flowing
112 through Tan Trung commune, Phu Tan district (right bank), and My Hoi Dong and Kien An communes, Cho Moi
113 district (left bank), An Giang Province, was licensed with the objectives of reducing bank erosion and supplying sand
114 for expressway construction projects ([An Giang Provincial People’s Committee 2023](#)).



115

116

Figure 1 a) Topo DEM in Mekong Delta include the study area ([Minderhoud et al. 2019](#)) b) Study area

117

The sand mining site is located along the Vam Nao River, adjacent to Phu Tan commune on the right bank and Cho Moi and Nhon My communes on the left bank in An Giang Province (see Figure 1b). The mining area covers 79.9 ha, with a mining reach length of approximately 4.778 km. The planned extraction period is three years, with an average dredging capacity of 1,200,000 m³ per year and a maximum allowable bed elevation of -15 m ([An Giang Provincial People’s Committee 2023](#)).

120

122 3. METHODS

123 3.1. Methodological framework

124

Figure 2 presents the methodological framework of the study, which consists of four main steps. In Step 1, data preparation, riverbanks were delineated from Google Earth (GE), while riverbed topography was updated using survey data collected in 2022. Hydrological and sediment related data, including discharge (Q), water level (H), and total suspended sediment concentration (TSS), were extracted from the MIKE 11 model and used as input for the HYDIST model. The second step involves the setup of the HYDIST model, comprising two components: the hydrodynamic model and the sediment transport model. The hydrodynamic model provides velocity fields (U, V) and bed shear stress (τ_b), which serve as inputs for sediment transport simulations. This is followed by the model calibration and validation stage, during which simulated results are compared with observed data to assess model reliability. Finally, the validated model is applied to analyze morphological changes under three scenarios: (i) the baseline condition, (ii) sand mining, and (iii) sand mining combined with climate change impacts. These scenarios enable a combined assessment of the effects of anthropogenic activities and climatic factors on the evolution of riverbed morphology.

134

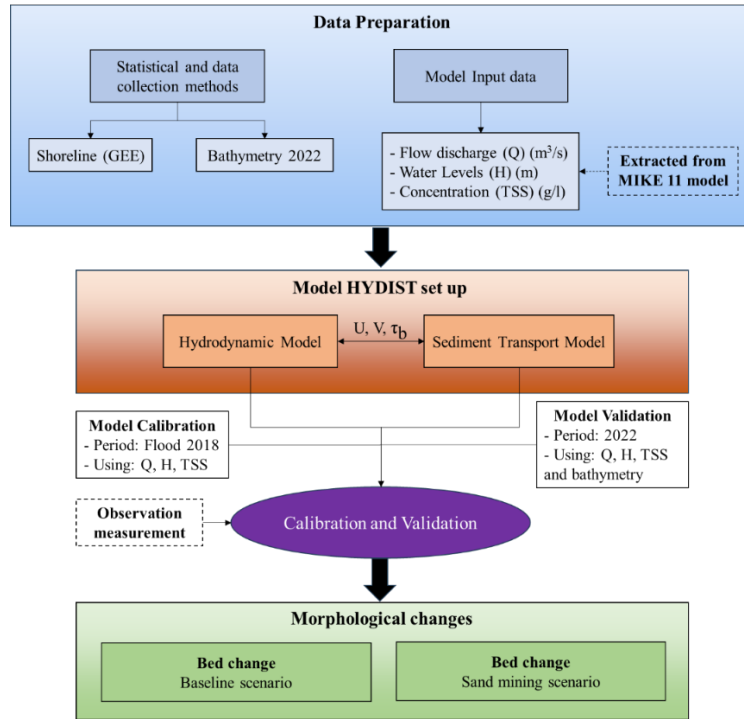


Figure 2 Methodological Framework in this study

3.2. Materials

Boundary data of discharge $Q(t)$ and $\zeta(t)$ for the years 2018 and 2022 were inherited from the MIKE 11 model developed under the project “Study on identifying causes and mechanisms and proposing technically feasible and economically effective solutions to mitigate erosion and deposition in the river system of the Mekong Delta (KH-CN-TNB.DT/14-19/C10)” (Bay 2017 - 2021).

Hourly discharge (Q) and water level (H) data, together with daily suspended sediment concentration (TSS) data for 2018 and 2022 at the Vam Nao station, were collected from the Southern Regional Hydro-Meteorological Center and used for model calibration and validation.

Bathymetric data and information on sand mining sites were obtained from the project “Dredging and river training of the Vam Nao River to mitigate bank erosion in My Hoi Dong commune and Kien An commune, Cho Moi district, An Giang Province” (Department of Science and Technology of An Giang Province 2023).

Grain size distribution data were inherited from the project “Study on identifying causes and mechanisms and proposing technically feasible and economically effective solutions to mitigate erosion and deposition in the river system of the Mekong Delta (KH-CN-TNB.DT/14-19/C10)” (Bay 2017 - 2021). Sediments in the study area are non-cohesive sand-silt material, with $d_{50} = 0.05$ mm and $d_{90} = 0.1$ mm.

3.3. HYDIST model

The HYDIST model is a 2D surface model, in which the O_x and O_y axes represent the longitudinal and transverse directions of the study area, as illustrated in **Error! Reference source not found.**. The model is formulated based on four governing equations: the depth-averaged Reynolds equations, the continuity equation, the sediment diffusion and transport equation, and the bed evolution continuity equation (Kim et al. 2020).

3.3.1. Reynolds Equation in the O_x and O_y Directions

$$\frac{\partial u}{\partial t} + u \frac{\partial u}{\partial x} + v \frac{\partial u}{\partial y} = -g \frac{\partial \zeta}{\partial x} - Ku \frac{\sqrt{u^2 + v^2}}{h + \zeta} + A \nabla^2 u \quad (3.1)$$

$$\frac{\partial v}{\partial t} + u \frac{\partial v}{\partial x} + v \frac{\partial v}{\partial y} = -g \frac{\partial \zeta}{\partial y} - K v \frac{\sqrt{u^2 + v^2}}{h + \zeta} + A \nabla^2 v \quad (3.2)$$

$$\frac{\partial \zeta}{\partial t} + \frac{\partial}{\partial x} [(h + \zeta)u] + \frac{\partial}{\partial y} [(h + \zeta)v] = 0 \quad (3.3)$$

158 3.3.2. Suspended Sediment Transport Equation

$$\frac{\partial C}{\partial t} + \gamma_v \left(u \frac{\partial C}{\partial x} + v \frac{\partial C}{\partial y} \right) = \frac{1}{H} \frac{\partial}{\partial x} \left(H K_x \frac{\partial C}{\partial x} \right) + \frac{1}{H} \frac{\partial}{\partial y} \left(H K_y \frac{\partial C}{\partial y} \right) + \frac{S}{H} \quad (3.4)$$

159 Where: S is the source term representing the rate of deposition and erosion (m/s). The source term is defined
160 according to the empirical formulation proposed by Van Rijn ([Van Rijn 1993](#)):

161 + When the bed shear stress exceeds the critical shear stress for erosion: $\tau_b > \tau_e$, S is an erosion function and S
162 = E:

$$E = \frac{M}{\rho_s} \frac{\tau_b - \tau_e}{\tau_e} \quad (3.5)$$

163 + When the bed shear stress is lower than the critical shear stress for deposition: $\tau_b < \tau_d$, S is a deposition
164 function and S = D:

$$D = -\omega_{sm} C_b \frac{\tau_d - \tau_b}{\tau_d} \quad (3.6)$$

165 + When $\tau_e \geq \tau_b \geq \tau_d$:

$$S = 0 \quad (3.7)$$

166 3.3.3. Bed Load Continuity Equation with Sand Mining Component

$$\frac{\partial h}{\partial t} = \frac{1}{1 - \varepsilon_p} \left[(S + S_{sm}) + \frac{\partial}{\partial x} \left(H K_x \frac{\partial C}{\partial x} \right) + \frac{\partial}{\partial y} \left(H K_y \frac{\partial C}{\partial y} \right) + \frac{\partial q_{bx}}{\partial x} + \frac{\partial q_{by}}{\partial y} \right] \quad (3.8)$$

167 Where: S_{sm} is the sand mine source and the standing sand mining rate (m/s).

168 The above equations are solved using the finite difference method with the Alternating Direction Implicit (ADI)
169 scheme proposed by Peaceman and Rachfor ([Kim et al. 2020](#)).

170 3.4. Model Performance Assessment

171 In this study, the quality of model calibration and validation is evaluated using the indicators R^2 , NSE, RSR, and
172 PBIAS. Specifically, R^2 represents the degree of linear correlation, NSE evaluates how well the simulated values
173 match the observed data relative to the variance of the observations, RSR reflects the relative magnitude of errors, and
174 PBIAS indicates the tendency of the model to overestimate or underestimate compared with observed data ([Moriasi
175 et al. 2015](#)). The indexes R^2 , NSE, RSR, and PBIAS are calculated using Eqs. (3.9 – 3.12). The performance rating
176 criteria for these indexes are summarized in Table 1.

$$R^2 = \left[\frac{\sum_{i=1}^n (O_i - \bar{O})(P_i - \bar{P})}{\sqrt{\sum_{i=1}^n (O_i - \bar{O})^2} \sqrt{\sum_{i=1}^n (P_i - \bar{P})^2}} \right]^2 \quad (3.9)$$

$$NSE = 1 - \frac{\sum_{i=1}^n (O_i - P_i)^2}{\sum_{i=1}^n (O_i - \bar{P})^2} \quad (3.10)$$

$$RSR = \frac{RMSE}{STDEV_{obs}} = \frac{\sqrt{\frac{1}{n} \sum_{i=1}^n (O_i - P_i)^2}}{\sqrt{\frac{1}{n} \sum_{i=1}^n (O_i - \bar{P})^2}} \quad (3.11)$$

$$PBIAS (\%) = \frac{\sum_{i=1}^n (O_i - P_i)}{\sum_{i=1}^n P_i} \times 100 \quad (3.12)$$

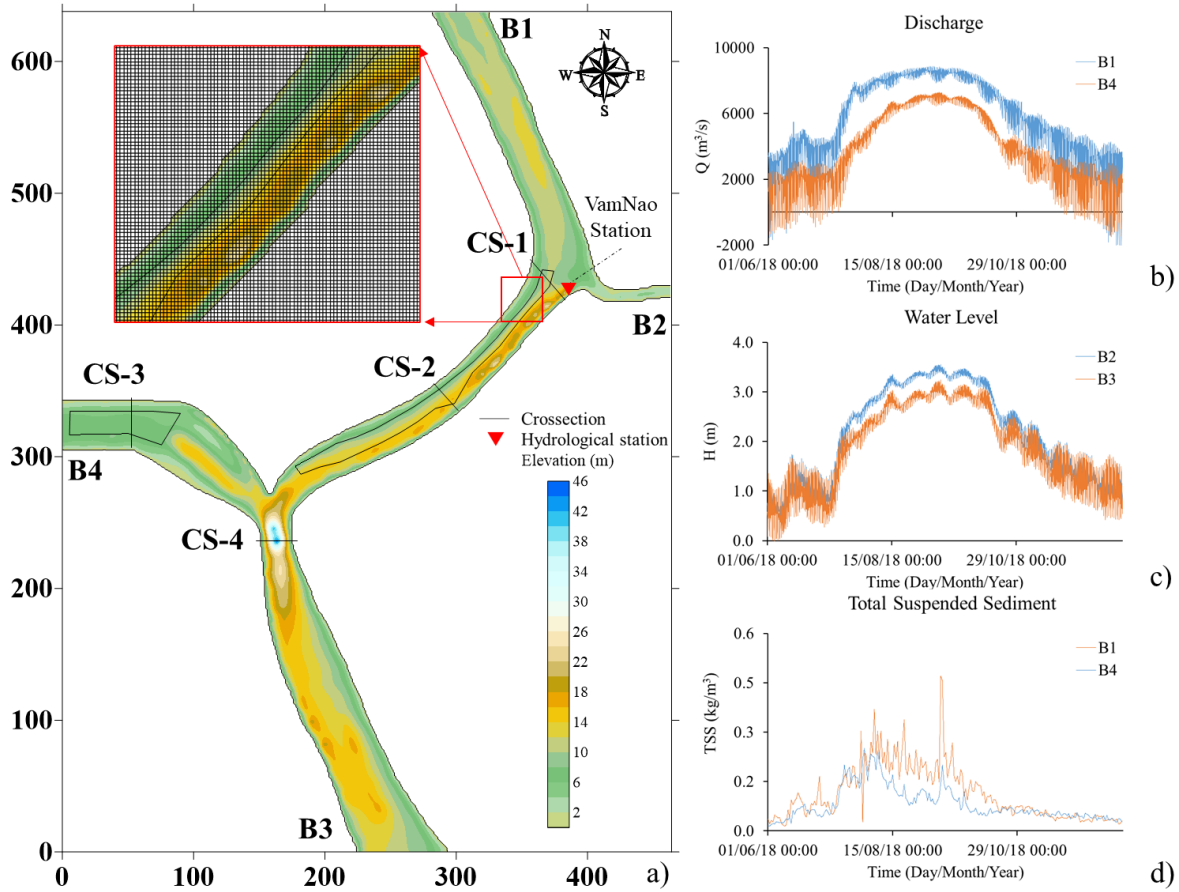
177 **Table 1** R², RSR, NSE and PBIAS general performance ratings for recommended statistics ([Moriasi et al. 2015](#))

Hydraulics and sediment			
Performance	R²	NSE	RSR
Very Good	R ² > 0,80	0,75 < NSE ≤ 1,00	0 ≤ RSR ≤ 0,50
Good	0,70 ≤ R ² ≤ 0,80	0,65 < NSE ≤ 0,75	0,50 ≤ RSR ≤ 0,60
Satisfactory	0,50 ≤ R ² ≤ 0,70	0,50 < NSE ≤ 0,65	0,60 ≤ RSR ≤ 0,70
Unsatisfactory	R ² ≤ 0,50	NSE ≤ 0,50	RSR > 0,70
Morphology			
PBIAS			
Very Good	PBIAS < 10		
Good	10 ≤ PBIAS < 15		
Satisfactory	15 ≤ PBIAS < 20		
Unsatisfactory	PBIAS > 20		

178 **4. SET UP MODEL**

179 **4.1. Mesh**

180 The computational mesh for the Vam Nao River reach is a rectilinear grid consisting of 636 × 462 cells, covering both
 181 the river channel and land areas. The maximum water depth represented in the mesh is h = 43.45 m, with structure
 182 grid spacing of Δx = Δy = 20 m. Sand mining locations are incorporated into the model in the form of a source matrix
 183 S_{sm} (i, j) with the same dimensions as the computational grid (see Figure 3b), where S_{sm} (i, j) represents the sand
 184 extraction rate at each grid cell (i, j). The sand mining rate at each cell (i, j) is calculated based on field data obtained
 185 from the project documentation ([Department of Science and Technology of An Giang Province 2023](#)), and is
 186 summarized in Table 2. In contrast to the approach adopted by Tran Thi Kim et al. (2020) ([Kim et al. 2020](#)), the present
 187 study determines the average sand mining rate from actual operating time records and then assumes continuous
 188 extraction to assess the impacts of sand mining on riverbed morphology.



189

190 **Figure 3** a) Riverbed topography in 2022 and the HYDIST computational mesh; b) discharge data; c) water level;
 191 and d) suspended sediment concentration extracted from the MIKE 11 model

192

Table 2 Average exploitation speed of sand mines

Sand mine	Extractable volume (m ³)	Area (m ²)	Mining rate (m/s)	Working time (hours)	Mine lifetime (years)
Vam Nao	3,461,000	799,000	1.22x10 ⁻⁷	9 hours	3 years
Binh Thuy	4,161,213	614,700	1.87x10 ⁻⁷	9 hours	2 years

193

4.2. Boundary data and initial condition

194

4.2.1. Initial conditions

195

196

197

198

In the model, when computations start at $t_0 = 0$, the hydrodynamic problem is initialized with a static condition over the entire domain. In cases where the simulation is continued from a given time $t = t_1$, the initial conditions consist of the velocity fields $u, v(x, y)$ and the sediment concentration field $C(x, y)$ at time t_1 over the whole computational domain.

199

4.2.2. Boundaries conditions

200

Hydrodynamic conditions:

201

202

The upstream and left boundaries are prescribed using the discharge time series $Q(t)$ and the velocity distribution along the open boundaries is redistributed according to the following formula:

$$u, v = \left[\frac{\frac{Q}{\sum(h_i^3)} h_i^{\frac{5}{3}}}{h_i \Delta x} \right] \quad (3.13)$$

203 The downstream and right boundaries are defined using the water level time series $z(t)$.

204 Sediment transport conditions:

205 When flow enters the computational domain, the sediment concentration is set to $C = C_0$.

206 When flow exits the domain, sediment concentration is computed through advective transport, with diffusion
207 neglected, and solved using the method of characteristics (Bay et al. 2019). With this approach, sediment is allowed
208 to enter and leave the computational domain, leading to more accurate simulation results.

209 **Land boundary:**

210 Hydrodynamics conditions: $u_n = 0$

211 Sediment transport conditions: $\frac{\partial c}{\partial n} = 0$

212 The Vam Nao station is used for model calibration and validation. This study employs the 2018 flood season
213 and both the dry season and flood season of 2022 for calibration and validation. Input data include discharge $Q(t)$,
214 water level $\zeta(t)$ and sediment concentration $C(t)$ for the years 2018 and 2022, as shown in Figure 3b, c, d.

215 **4.3. Model parameter**

216 The model parameters used in this study are presented in Table 3. In which, the median grain size (d_{50}) and the
217 characteristic grain size (d_{90}) were determined from sediment samples measured in situ in the study area (Bay 2017 -
218 2021). Other parameters such as porosity, particle density, kinematic viscosity, and critical deposition–erosion shear
219 stress were inherited from previous studies and adjusted during the model calibration process (Binh et al. 2022; Thanh
220 et al. 2017; Hung et al. 2014).

221 **Table 3** Parameter of the HYDIST model

Parameters	Value
Time step Δt	2 (s)
Roughness coefficient n	0.015 – 0.027
Particle porosity ε_p	0,375
Median particle diameter (d_{50}) 50%	5×10^{-5} (m)
Particle diameter (d_{90}) 90%	1×10^{-4} (m)
Kinematic viscosity (ν)	$1,01 \times 10^{-6}$ (m ² /s)
Particle density (ρ_s)	2600 (kg/m ³)
Erosion coefficient M	1×10^{-6} (kg/m ² /s)
Critical deposition shear stress τ_d	0,06 (N/m ²)
Critical erosion shear stress τ_e	0,35 (N/m ²)

222 **4.4. Scenarios**

223 In this study, simulation scenarios were developed to comprehensively evaluate the factors governing riverbed
224 morphological changes in 2022. Based on Decision No. 1541/QD-UBND approving the list of river sand mineral areas
225 serving infrastructure development and socio-economic projects in the Mekong Delta, the Vam Nao river reach was

226 identified as one of the important sand mining sites of An Giang province ([An Giang Provincial People’s Committee](#)
 227 [2023](#)). However, this area simultaneously exhibits complex hydraulic–morphological conditions and frequently
 228 experiences severe bank erosion, raising concerns that sand mining activities may increase the risk of channel
 229 instability. On this basis, the study established two simulation scenarios to analyze and evaluate the riverbed
 230 morphological evolution at Vam Nao. In which, scenario KB-1 represents the existing condition without sand mining
 231 and serves as the reference scenario, while scenario KB-2 incorporates the impacts of sand mining activities to quantify
 232 the level of influence on channel morphology changes, particularly the variation of scour holes at the confluence of
 233 the Vam Nao River reach.

Scenario name	Description
SC-1	Simulation of riverbed evolution in 2022 under existing conditions (no sand mining).
SC-2	Simulation of riverbed evolution in 2022 with the Vam Nao sand mine and the Binh Thuy sand mine.

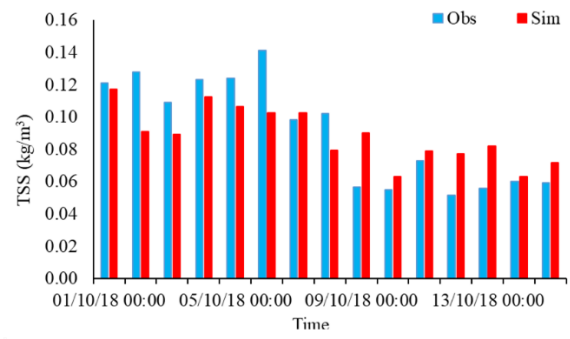
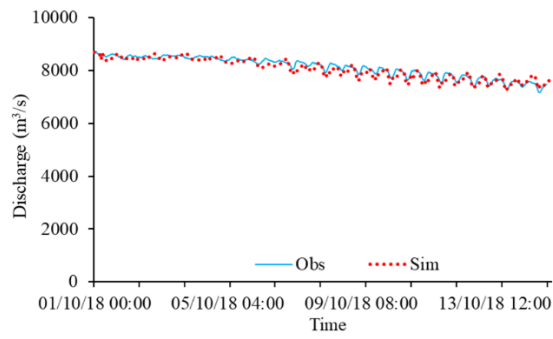
234 5. RESULTS

235 5.1. Calibration and validation model

236 The model was calibrated and validated using data from the flood season in 2018, and the dry season and flood season
 237 in 2022. This study focused on simulating one flood season year (from June to December) in order to reduce simulation
 238 time, since more than 90% of suspended sediment load is transported during the flood season ([Binh et al. 2020](#)).
 239 Measured data at the Vam Nao station were used for model calibration and validation, including discharge, water level,
 240 suspended sediment, and three cross sections of the Vam Nao River. In sequence, the hydraulic model was first
 241 calibrated by adjusting the roughness coefficient. Subsequently, the bed sediment transport model was further
 242 calibrated through the erosion coefficient M , critical deposition shear stress τ_d and critical erosion shear stress τ_e . The
 243 calibration and validation results of the parameters met acceptable criteria, specifically the roughness coefficient n
 244 ranged from $0,0145 - 0,0275 \text{ s/m}^{1/3}$, the erosion coefficient $M = 2 \times 10^{-5} \text{ (kg/s.m}^2\text{)}$, the critical deposition shear stress
 245 $\tau_d = 0,04 \text{ (N/m}^2\text{)}$ and the critical erosion shear stress $\tau_e = 0,15 \text{ (N/m}^2\text{)}$. The values of R^2 , RMSE, NSE và PBIAS (Table
 246 4) indicate that the HYDIST model was calibrated and validated in a reliable manner. Furthermore, the simulated
 247 discharge, water level, TSS, and riverbed depth are consistent with the corresponding measured data (Figure 4 and
 248 Figure 5) ([Moriassi et al. 2015](#)).

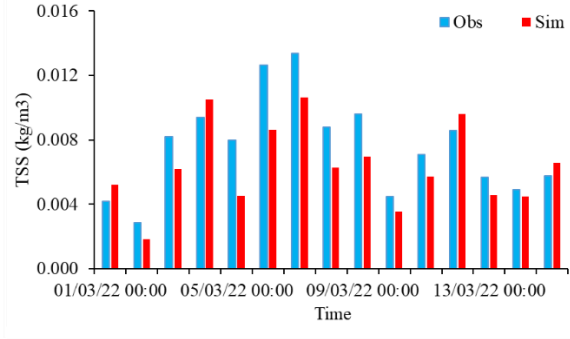
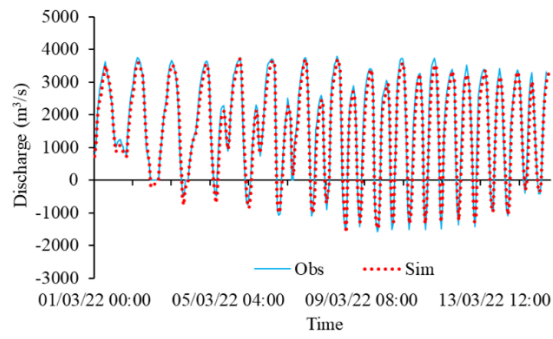
249 **Table 4** Evaluation of the model performance

Values	Model Calibration		Model Validation			
	Flood 2018	Dry 2022	Flood 2022	CS - 1	CS - 2	CS - 3
Discharge	R^2	0.88	0.84	0.70		
	NSE	0.86	0.83	0.55		
	RSR	0.36	0.40	0.66		
Water Level	R^2	0.88	0.91	0.91		
	NSE	0.81	0.90	0.90		
	RSR	0.37	0.31	0.31		
TSS	R^2	0.61	0.69	0.55		
	NSE	0.53	0.51	0.54		
	RSR	0.66	0.67	0.65		
Cross-section	PBIAS			13.53	11.35	20.02



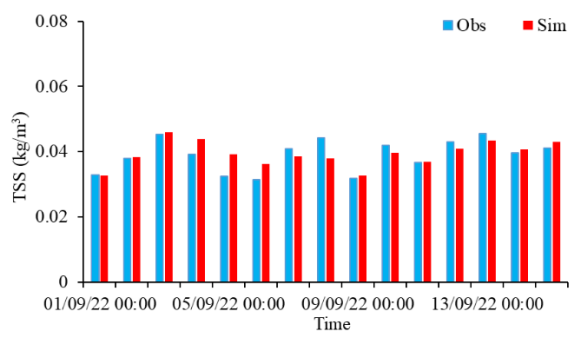
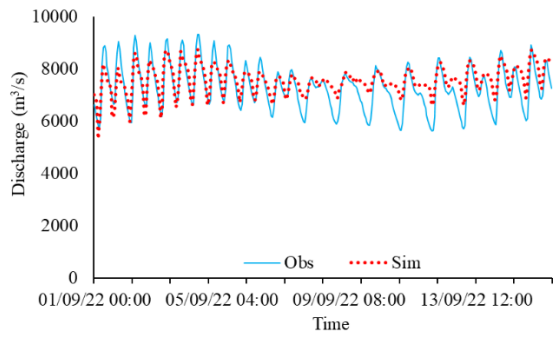
a)

e)



b)

f)



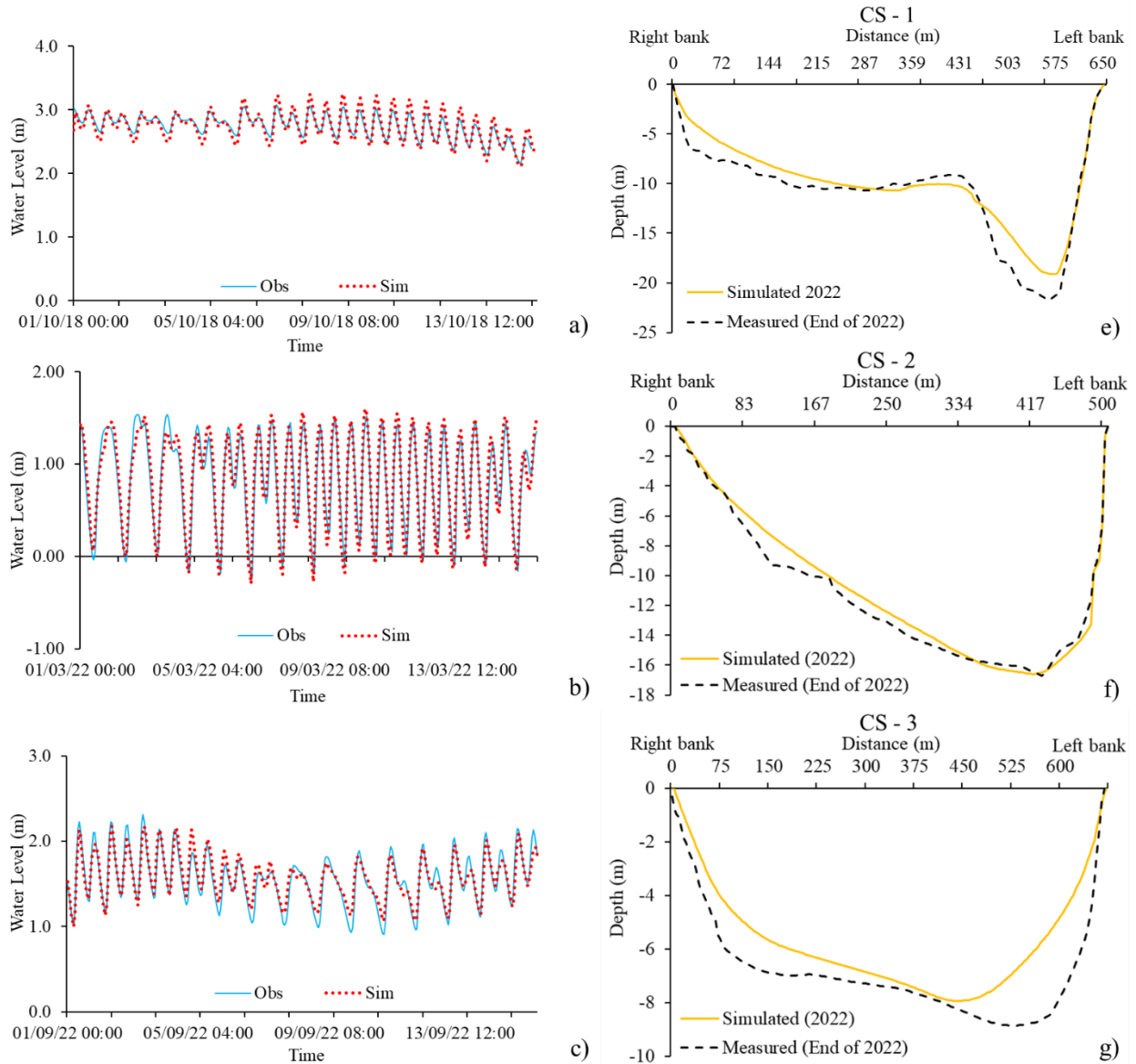
c)

g)

250

251

Figure 4 Calibration and validation of discharge and suspended sediment



252

253

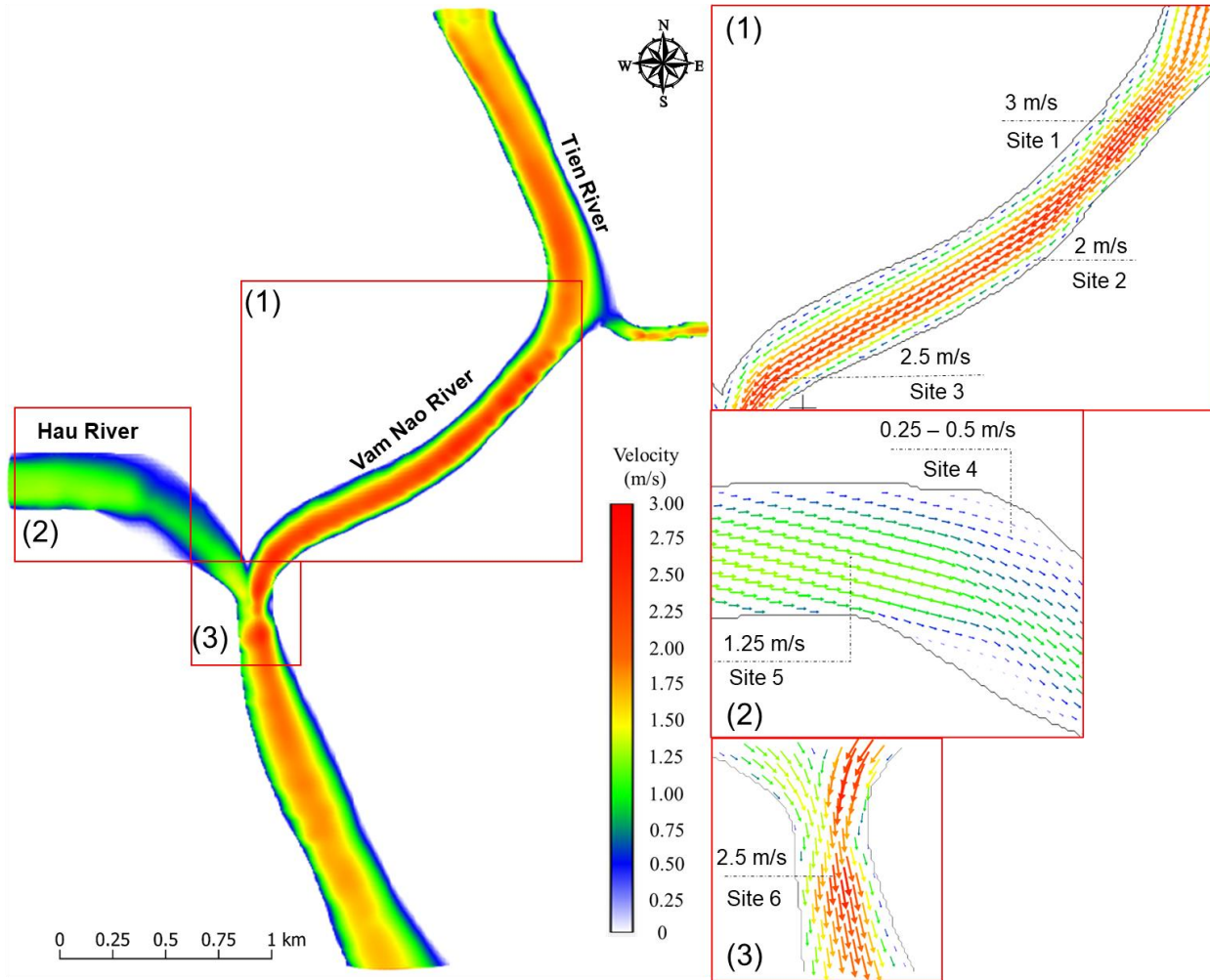
Figure 5 Calibration and validation of water level and cross sections

254 **5.2. Hydrodynamic in the Vam Nao River confluence**

255 The hydrodynamic simulation results at the flood peak at 20:00 on 01/10/2022 are presented in Figure 6, illustrating
 256 the spatial distribution of the flow velocity field in the study area and indicating pronounced heterogeneity in
 257 hydrodynamic conditions. Specifically, the Vam Nao River reach plays the role of a water transfer pathway from the
 258 Tien River to the Hau River, characterized by a high velocity flow field. In Zone 1, the flow within the Vam Nao
 259 channel reaches a maximum velocity of up to 3.0 m/s at location 1 (concave bank area) and ranges from 2.0 – 2.5 m/s
 260 at locations 2 and 3. The velocity vectors in this area are highly concentrated and exhibit large magnitudes, reflecting
 261 the strong kinetic energy of flow transferred from the Tien River to the Hau River.

262 In contrast, in Zone 2 located in the upstream reach of the Hau River, the velocity field records significantly
 263 lower values, ranging only from 0.25 – 0.5 m/s at location 4 near the riverbank and approximately 1.0 m/s at location
 264 5 in the middle of the channel. The large disparity in velocity fields between the Vam Nao flow and the upstream flow
 265 of the Hau River creates a complex hydraulic interaction zone at the river confluence (Zone 3). At this location

266 (location 6), the confluence leads to a localized increase in flow velocity (reaching 2.5 m/s), generating turbulent flows
 267 that are capable of inducing bank failure, deep scour, and severe changes in channel morphology.



268
 269 **Figure 6** Velocity field at flood peak at 20:00 on 01/10/2022

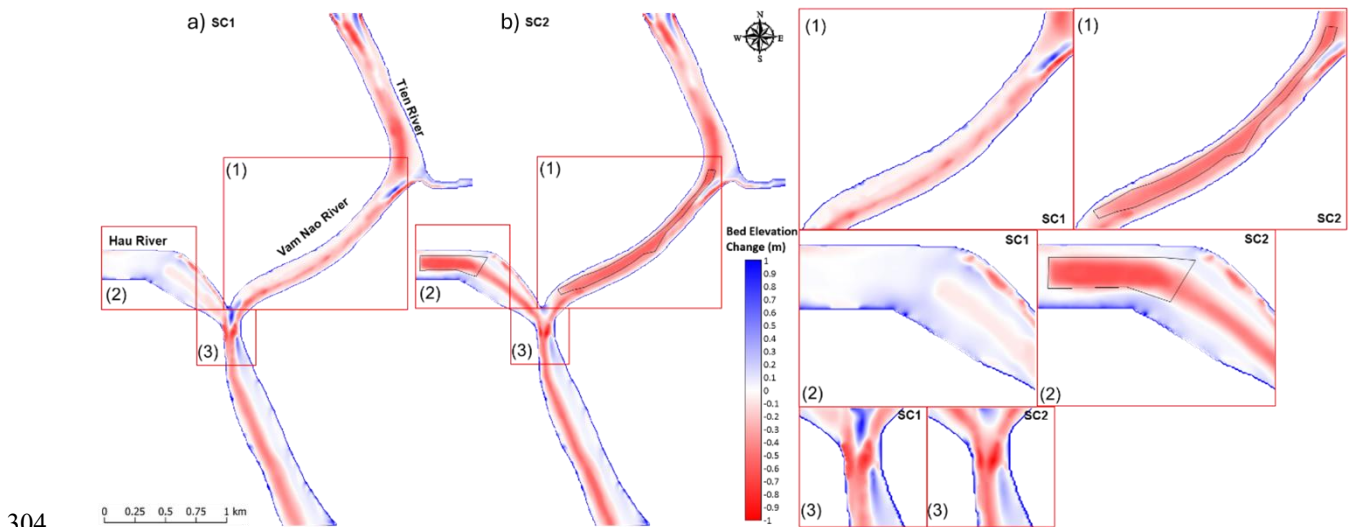
270 **5.3. Bed change in Vam Nao with sand mining and without sand mining**

271 Figure 7 shows a clear contrast in bed elevation evolution between the two scenarios. Under SC2, sand mining
 272 activities markedly intensify erosion compared to the existing condition, with deep scour zones forming directly within
 273 the mining areas in both Zone 1 and Zone 2. Due to changes in the velocity field after the flow passes through the
 274 mining sites in the Hau River and the Vam Nao River, erosion is not confined to the extraction locations but propagates
 275 downstream, most clearly expressed in Zone 3, corresponding to the Hau–Vam Nao confluence. In this zone, erosion
 276 develops asymmetrically toward the right bank and exhibits substantially greater intensity under scenario SC2. In
 277 Zone 1, the baseline scenario (SC1) indicates that this river reach is already dominated by erosional conditions, with
 278 erosion accounting for 72.9% of the total bed change (equivalent to 426,153 m³). However, under the mining scenario
 279 (SC2), sediment imbalance becomes more severe. The data indicate a pronounced reduction in deposition, decreasing
 280 from 27.1% (158,561.87 m³) to only 12.9% (124,180.10 m³), while erosion increases sharply, accounting for 87.1%
 281 of the total bed change. Notably, the total volume of material lost under SC2 reaches approximately 840,849.06 m³,
 282 nearly doubling (about 1.97 times) that of the baseline scenario, which is only 426,152.71 m³.

283 In contrast to the strong hydraulic regime of the Vam Nao River, the Hau River area (Zone 2) under natural
 284 conditions exhibits characteristics of a sediment deposition environment. Specifically, in the baseline scenario (SC1),

285 this area functions as a sediment trap, with deposition overwhelmingly dominant (83.77%, equivalent to 256,993.19
 286 m³), while erosion remains negligible. However, sand mining activities under SC2 completely reverse this bed
 287 evolution trend. From a depositional state, the area shifts to a strongly erosional regime, with erosion becoming
 288 dominant at 68.81% (reaching 416,930.3 m³). Remarkably, the erosion volume in this scenario increases by a factor
 289 of 8.4 compared to natural conditions (49,783 m³).

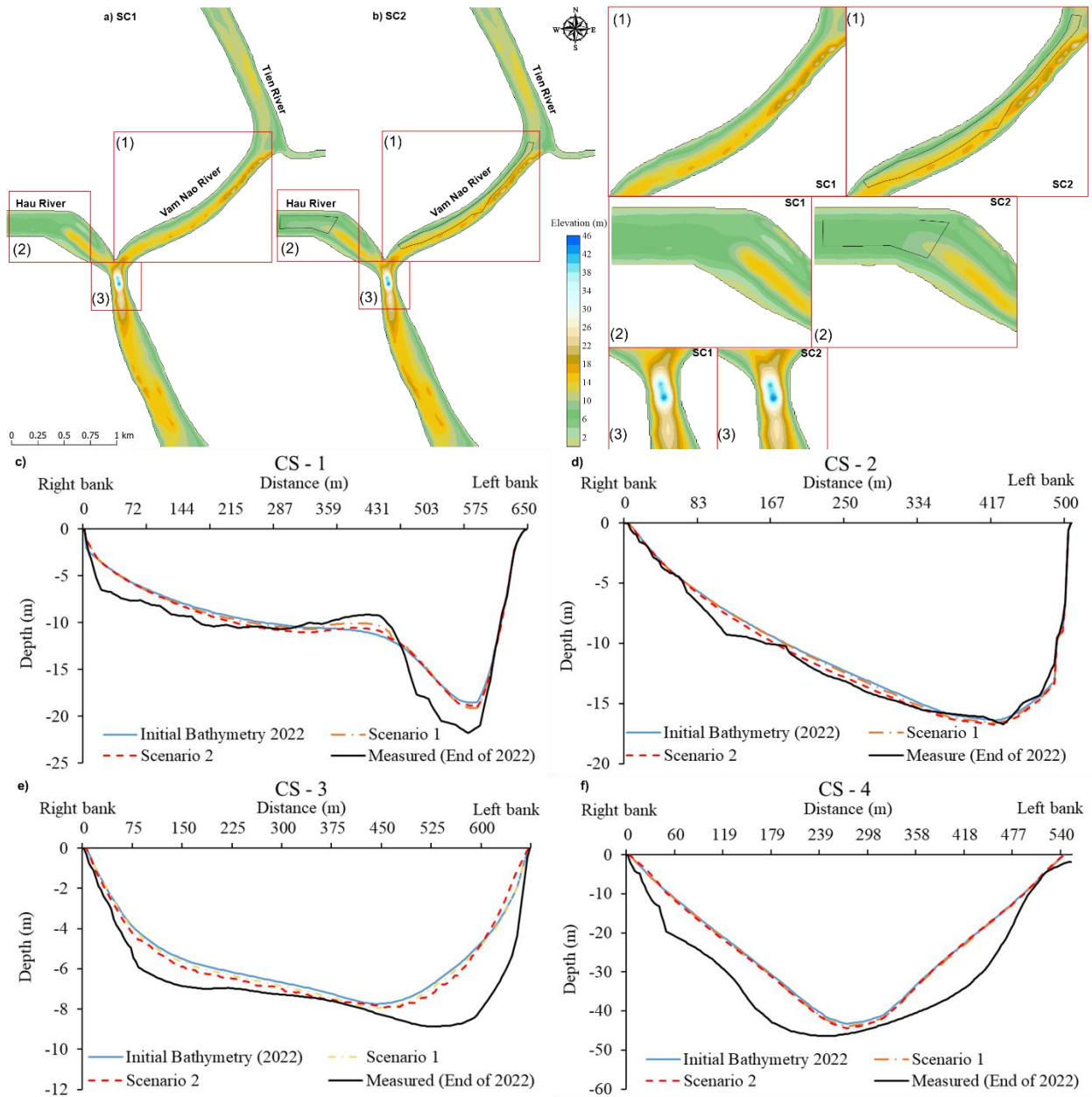
290 The river confluence area (Zone 3), a hydraulic junction where complex flow interactions occur between the
 291 Tien River (via the Vam Nao reach) and the Hau River, exhibits a high sensitivity to upstream alterations. Under the
 292 baseline scenario (SC1), this zone maintains a state in which erosion is dominant, accounting for approximately
 293 58.63% (149,761.11 m³) of the total morphological change due to the presence of a naturally developed deep scour
 294 hole, while still sustaining a substantial proportion of deposition at about 41.37% (105,673.38 m³). However, scenario
 295 SC2 alters both the dynamic processes and the morphological behavior of the area. The results indicate a severe
 296 reduction in deposition, decreasing by 30.2% in volume compared to SC1, while erosion intensifies to represent
 297 69.56% of the total morphological change. The increase in total erosion volume (rising by about 12.5% to reach
 298 168,435 m³) in Zone 3 provides clear evidence of a propagating impact. Upstream dredging activities in Zones 1 and
 299 2 retain a large proportion of bed sediment, leading to a condition of sediment starvation at the river confluence. As a
 300 consequence, the flow in this already complex interaction zone is forced to increase its erosive energy locally to
 301 compensate for the material deficit, thereby elevating the risk of bank instability and further expansion of scour holes.
 302 This finding confirms that localized dredging interventions can induce adverse morphological effects that propagate
 303 downstream, threatening the stability of river training structures and riverbanks at vulnerable locations.



304
 305 **Figure 7** Comparison of bed layer thickness under a) no sand mining and b) sand mining scenarios

306 Figure 8c-f presents a comparison between the simulated bed topography under the two scenarios and the cross
 307 sections measured at the end of 2022 at four locations, CS-1, CS-2, CS-3 and CS-4. Overall, the model reproduces the
 308 general channel trends reasonably well, particularly the variation in depth toward the thalweg and the asymmetric
 309 geometric form governed by flow concentration. At CS-1 (Figure 8c), erosion is concentrated along the left bank in
 310 both scenarios; however, the sand mining scenario exhibits deeper scour in the reach from 144–359 m and a noticeable
 311 shift of the erosional zone toward the channel center. The simulated results are consistent in trend with the measured
 312 bed topography in 2022. At CS-2 (Figure 8d), erosion is focused in the central part of the channel, with depths under
 313 the sand mining scenario exceeding those of the no-mining scenario by 0.8–1.0 m. At CS-3 (Figure 8e), the simulation
 314 successfully captures the deepening trend toward the right bank and the asymmetric channel shape, with maximum
 315 depths ranging from –7.2 to –7.8 m compared to the measured value of –10.5 m, indicating that the model adequately
 316 represents the overall direction of morphological change. The CS-4 cross section clearly illustrates bed lowering

317 within the scour hole area under the influence of dredging activities, while the asymmetric V-shaped channel form is
 318 maintained (Figure 8f).



319
 320 **Figure 8** Comparison of bed topography evolution under a) no sand mining, b) sand mining scenarios and four
 321 crosssection (c-f)

322 Specifically, relative to the baseline scenario (SC1), the maximum bed elevation in the dredging scenario (SC2)
 323 is further lowered by approximately 2.0 m, reaching a depth of about -45 m compared to -43 m under existing
 324 conditions, directly reflecting anthropogenic intervention in the channel profile. Overall, sand mining distinctly alters
 325 the spatial distribution of erosion and deposition, promotes the development of new flow paths, and reduces direct
 326 impacts on the riverbanks. The simulation results obtained in this study show strong agreement with recent field
 327 observations reported by Vu et al. (2025) (Vu et al. 2025). Based on measured data, these authors documented a trend
 328 of deepening and downstream expansion of the scour hole at the river confluence. The successful reproduction of this

329 morphological evolution by the model not only reinforces the reliability of the simulation scenarios but also provides
330 quantitative evidence supporting the conclusion that sand mining activities are a key driver intensifying scour
331 development at the confluence area.

332 6. DISCUSSION

333 The simulation results for the Vam Nao River reach demonstrate that sand mining activities exert a pronounced
334 influence on channel morphological evolution. A comparison between the scenarios with and without sand mining
335 indicates that, in the Vam Nao area (Zone 1), the proportion of deposition decreases from 27.1% to 12.9% under the
336 mining scenario, while erosion accounts for as much as 87.1% of the total morphological change. Notably, in the Hau
337 River reach (Zone 2), which is naturally characterized by depositional conditions, erosion increases abruptly, with the
338 total eroded volume approximately 8.4 times greater than that under the no-mining scenario. In the Vam Nao–Hau
339 River confluence area (Zone 3), deposition volume decreases by 30.2% relative to the condition without sand mining,
340 while erosion represents 69.56% of the total morphological change, clearly indicating a downstream propagating
341 impact of upstream sand extraction.

342 These findings are consistent with general trends reported in numerous international studies on in-channel sand
343 mining. Global syntheses have consistently identified sand extraction as a major driver of riverbed lowering, channel
344 widening, and increased bank instability ([Rentier and Cammeraat 2022](#); [Binh et al. 2022](#); [Kim et al. 2020](#); [Padmalal
345 and Maya 2014a](#)). In particular, studies conducted within the Mekong River basin indicate that current sand extraction
346 volumes far exceed the natural replenishment capacity of the system, resulting in widespread sediment deficits ([Gruel
347 et al. 2022](#); [Hackney et al. 2020a](#)). This context explains why, in the present study, although mining areas occupy only
348 a limited portion of the channel, their morphological impacts extend downstream to the confluence reach.

349 The results of this paper also show strong agreement with previous field-based and remote sensing studies
350 conducted in the Mekong Delta, which have documented progressive riverbed deepening, expansion of scour holes,
351 and temporal shifts of the thalweg in river reaches heavily affected by sand mining ([Vu et al. 2025](#); [Binh et al. 2022](#)).

352 When compared with detailed modeling and observational studies conducted on river reaches affected by sand
353 mining, the magnitudes of local scour at Vam Nao fall within a comparable range but exhibit higher intensity. Kim et
354 al. (2020) reported riverbed lowering rates of 0.6 to 1.2 m/year along reaches of the Tien River directly influenced by
355 sand mining ([Kim et al. 2020](#)). In the present study, results at cross section CS-2 indicate that bed depth under the
356 sand mining scenario exceeds that of the no-mining scenario by 0.8–1.0 m within only one simulated year, while in
357 the deep scour area (CS-4), the riverbed elevation decreases by an additional 2.0 m (from about –43 m to nearly –45
358 m). This indicates that erosion intensity at Vam Nao is generally comparable to that observed along the segment of
359 Tien River flowing Tan Chau, and at certain scour locations it even exceeds it. Nguyen Nghia Hung et al. (2020)
360 reported an average riverbed lowering rate across the Mekong Delta of approximately 15.3 cm/year during the period
361 2008–2018 ([Hung et al. 2020](#)), while Hackney et al. (2020) estimated a rate of about 0.13 m/year ([Hackney et al.
362 2020a](#)) c The study by Christopher R. Hackney et al. (2020) further demonstrated that unsustainable sand mining can
363 deepen channels and enlarge scour holes with amplitudes ranging from 1.5 to 3.0 m in sensitive reaches of the Mekong
364 River. The local scour depths observed at Vam Nao, particularly in the confluence area, lie within this range, indicating
365 that sand mining impacts at this site are not minor or isolated phenomena but belong to the category of high impact
366 cases documented across the region ([Hackney et al. 2020a](#)).

367 The study by ([Vu et al. 2025](#)) documented significant riverbed incision along the Hau River, with maximum
368 annual net erosion volumes reaching 29.48 million m³/year and average erosion rates of up to 0.82 m/year. In addition,
369 excessive sand mining activities resulted in the formation of 23 scour holes with depths of up to 11 m and caused
370 deepening of the main navigation channel (thalweg) at rates reaching –1.18 m/year during the period 2014–2023.
371 These findings are consistent with the quantitative results obtained for Vam Nao, where sand mining not only
372 intensifies erosion at the extraction sites but also leads to a pronounced reduction in deposition (a decrease of 30.2%)
373 and an increase in downstream propagating erosion (168,435 m³ within one year) at the confluence area, one of the
374 most critical hydrodynamic nodes of the Mekong River system.

375 Quantifying erosion and deposition volumes demonstrates that sand mining not only exacerbates erosion at
376 extraction sites but also substantially alters the morphological mechanisms of river reaches that are naturally
377 predisposed to deposition. The impact mechanism observed in this study is consistent with the concept of “hungry
378 water,” which has been widely discussed in international literature ([Hackney et al. 2020a](#); [Brunier et al. 2014](#); [Kondolf
379 1997](#)). When bed sediment is removed by mining activities, the flow becomes sediment-deficient, thereby increasing
380 its capacity to erode the channel bed and banks downstream in order to compensate for the sediment shortfall. In the
381 case of the Vam Nao River, sediment depletion caused by mining in Zones 1 and 2 enhances erosive energy at the
382 confluence area (Zone 3), where the flow field is already complex and characterized by high velocities. This explains
383 why the confluence exhibits a particularly high sensitivity to upstream anthropogenic interventions. Compared with
384 many previous modeling studies worldwide, which often assume fixed mining pits or consider morphological
385 responses only over long time intervals, the present study demonstrates that representing sand mining as a continuous,
386 time dependent process provides clearer insight into the dynamic nature of riverbed evolution. The results indicate
387 that within only one year of simulation, morphological changes are already sufficient to disrupt sediment balance
388 along several river reaches, especially at the confluence. This suggests that if sand extraction persists over multiple
389 consecutive years, the risk of channel instability and riverbank failure is likely to increase substantially.

390 **7. CONCLUSION**

391 The simulation results demonstrate that sand mining markedly intensifies erosion and disrupts the natural sediment
392 balance. In the Vam Nao River reach (Zone 1), the proportion of deposition decreases from 27.1% to 12.9%, while
393 erosion increases sharply, accounting for 87.1% of the total morphological change. This reflects a clear shift from a
394 relatively balanced erosion–deposition state toward an erosion dominated regime under the influence of sand mining.

395 In the Hau River reach (Zone 2), which under natural conditions functions as a sediment depositional
396 environment with deposition accounting for up to 83.77%, mining activities completely reverse the prevailing
397 morphological processes. The total erosion volume under the mining scenario reaches 416,930 m³, approximately 8.4
398 times greater than that observed in the no-mining scenario.

399 The most pronounced effects are observed at the Vam Nao–Hau River confluence (Zone 3), where the
400 downstream propagating impacts of upstream sand mining are clearly expressed. Under the mining scenario,
401 deposition volume in this area decreases by 30.2%, while erosion increases to 69.56% of the total morphological
402 change. Sediment starvation resulting from sediment being trapped at mining sites forces the flow at the confluence
403 to increase its local erosive energy, thereby enlarging and deepening existing scour holes and increasing the risk of
404 riverbank instability.

405 Nevertheless, this study is subject to several limitations. First, the model considers sand mining activities based
406 only on licensed extraction data and does not account for illegal or unreported mining, which is believed to be
407 widespread in the Mekong Delta and may substantially intensify actual erosion rates. Second, the study does not fully
408 incorporate the effects of climate change, including alterations in flow regimes, sea level rise, and reductions in
409 upstream sediment supply, all of which could further exacerbate long term morphological instability.

410 **FUNDING**

411 This research is funded by Vietnam National University Ho Chi Minh City (VNU-HCM) under a project within the
412 framework of the Program titled “Strengthening the capacity for education and basic scientific research integrated
413 with strategic technologies at VNU-HCM, aiming to achieve advanced standards comparable to regional and global
414 levels during the 2025–2030 period, with a vision toward 2045”.

415 **AUTHOR CONTRIBUTIONS**

416 Conceptualization: T.T.K and N.D.Q.H; methodology: T.T.K; software: T.T.K, and N.D.Q.H; writing—original draft
417 preparation: T.T.K and N.D.Q.H; writing—review and editing: T.T.K; visualization: T.T.K and N.D.Q.H; All authors
418 have read and agreed to the published version of the manuscript.

419 **CONFLICT OF INTEREST**

420 The authors declare that they have no known competing financial interests or personal relationships that could have
421 appeared to influence the work reported in this paper.

422 REFERENCE

- 423 An Giang Provincial Department of Natural Resources and Environment 2021 Results of riverbank failure monitoring
424 and warning in An Giang Province (Phase 1, 2021).
- 425 An Giang Provincial People's Committee (2023) *Decision No. 1541/QĐ-UBND: Approval of the list of sand source*
426 *areas serving expressway construction projects for the period 2023–2026, An Giang Province, Viet Nam.*
427 [Online], An Giang Province's Portal, Available: [https://angiang.gov.vn/vi/quyet-dinh-phe-duyet-danh-muc-](https://angiang.gov.vn/vi/quyet-dinh-phe-duyet-danh-muc-khu-vuc-khoang-san-cat-song-phuc-vu-nguon-vat-lieu-cho-cac-du-dau-tu)
428 [khu-vuc-khoang-san-cat-song-phuc-vu-nguon-vat-lieu-cho-cac-du-dau-tu](https://angiang.gov.vn/vi/quyet-dinh-phe-duyet-danh-muc-khu-vuc-khoang-san-cat-song-phuc-vu-nguon-vat-lieu-cho-cac-du-dau-tu) (Accessed 25/5/2025).
- 429 Anthony, E. J., Brunier, G., Besset, M., Goichot, M., Dussouillez, P. & Nguyen, V. L. (2015) Linking rapid erosion of
430 the Mekong River delta to human activities, *Sci Rep*, 5 (1), 14745. doi: <https://doi.org/10.1038/srep14745>.
- 431 Ashraf, M. A., Maah, M. J., Yusoff, I., Wajid, A. & Mahmood, K. (2011) Sand mining effects, causes and concerns: A
432 case study from Bestari Jaya, Selangor, Peninsular Malaysia, *Sci Res Essays*, 6 (6), 1216-1231. doi:
433 Barman, B., Kumar, B. & Sarma, A. K. (2018) Turbulent flow structures and geomorphic characteristics of a mining
434 affected alluvial channel, *Earth Surf Processes Landforms*, 43 (9), 1811-1824. doi:
435 <https://doi.org/10.1002/esp.4355>.
- 436 Barman, B., Kumar, B. & Sarma, A. K. (2019) Dynamic characterization of the migration of a mining pit in an alluvial
437 channel, *Int J Sediment Res*, 34 (2), 155-165. doi: <https://doi.org/10.1016/j.ijsrc.2018.10.009>.
- 438 Bay, N. T. 2017 - 2021 Research to identify causes, mechanisms and propose feasible technical and economic solutions
439 to reduce erosion, sedimentation for the Mekong river system (2017 – 2020), KHCN-TNB.ĐT/14-19/C10.
- 440 Bay, N. T., Kim, T. T., An, T. T. T. & Nga, T. N. Q. (2023) Assessing the impact of sand mining on the riverbed of the
441 Tien River flowing through Vinh Long Province, *Vietnam J Hydrometeorol*, 756, 14-28. doi:
442 [http://doi.org/10.36335/VNJHM.2023\(756\).14-28](http://doi.org/10.36335/VNJHM.2023(756).14-28).
- 443 Bay, N. T., Kim, T. T., Hoai, H. C. T., P.A., Huy, N. D. Q. & Phung, N. K. (2019) HYDIST model and the approach
444 of solving sediment concentration at open boundaries (in Vietnamese), *Vietnam J Hydrometeorol*, 704, 57-
445 64. doi: [http://doi.org/10.36335/VNJHM.2019\(704\).57-64](http://doi.org/10.36335/VNJHM.2019(704).57-64).
- 446 Binh, D. V., Kantoush, S. & Sumi, T. (2020) Changes to long-term discharge and sediment loads in the Vietnamese
447 Mekong Delta caused by upstream dams, *Geomorphology*, 353, 107011. doi:
448 <https://doi.org/10.1016/j.geomorph.2019.107011>.
- 449 Binh, D. V., Kantoush, S. A., Ata, R., Tassi, P., Nguyen, T. V., Lepesqueur, J., Abderrezzak, K. E. K., Bourban, S. E.,
450 Hung, N. Q. & Phuong, D. N. L. (2022) Hydrodynamics, sediment transport, and morphodynamics in the
451 Vietnamese Mekong Delta: Field study and numerical modelling, *Geomorphology*, 413, 108368. doi:
452 <https://doi.org/10.1016/j.geomorph.2022.108368>.
- 453 Bravard, J.-P., Goichot, M. & Gaillot, S. (2013) Geography of sand and gravel mining in the Lower Mekong River.
454 First survey and impact assessment, *EchoGéo*, (26). doi: <https://doi.org/10.4000/echogeo.13659>.
- 455 Brunier, G., Anthony, E. J., Goichot, M., Provansal, M. & Dussouillez, P. (2014) Recent morphological changes in the
456 Mekong and Bassac river channels, Mekong delta: The marked impact of river-bed mining and implications
457 for delta destabilisation, *Geomorphology*, 224, 177-191. doi:
458 <https://doi.org/10.1016/j.geomorph.2014.07.009>.
- 459 Dang, H. & Pokhrel, Y. (2024) Evolution of river regimes in the Mekong River basin over 8 decades and the role of
460 dams in recent hydrological extremes, *Hydrol Earth Syst Sci*, 28 (14), 3347-3365. doi:
461 <https://doi.org/10.5194/hess-28-3347-2024>.
- 462 Department of Science and Technology of an Giang Province 2023 Dredging and river training of the Vam Nao River
463 to mitigate riverbank erosion in My Hoi Dong Commune and Kien An Commune, Cho Moi District, An
464 Giang Province, Vietnam.
- 465 Farahani, H. & Bayazidi, S. (2018) Modeling the assessment of socio-economical and environmental impacts of sand
466 mining on local communities: A case study of Villages Tatao River Bank in North-western part of Iran, *Resour*
467 *Policy*, 55, 87-95. doi: <https://doi.org/10.1016/j.resourpol.2017.11.001>.

468 Gruel, C.-R., Park, E., Switzer, A. D., Kumar, S., Ho, H. L., Kantoush, S., Van Binh, D. & Feng, L. (2022) New
469 systematically measured sand mining budget for the Mekong Delta reveals rising trends and significant
470 volume underestimations, *Int J Appl Earth Obs Geoinf*, 108, 102736. doi:
471 <https://doi.org/10.1016/j.jag.2022.102736>.

472 Hackney, C. R., Darby, S. E., Parsons, D. R., Leyland, J., Best, J. L., Aalto, R., Nicholas, A. P. & Houseago, R. C.
473 (2020a) River bank instability from unsustainable sand mining in the lower Mekong River, *Nat Sustainability*,
474 3 (3), 217-225. doi: <https://doi.org/10.1038/s41893-019-0455-3>.

475 Hackney, C. R., Darby, S. E., Parsons, D. R., Leyland, J., Best, J. L., Aalto, R., Nicholas, A. P. & Houseago, R. C.
476 (2020b) River bank instability from unsustainable sand mining in the lower Mekong River, *Nature*
477 *Sustainability*, 3 (3), 217-225. doi: <https://doi.org/10.1038/s41893-019-0455-3>.

478 Hung, N. N., Delgado, J. M., Güntner, A., Merz, B., Bárdossy, A. & Apel, H. (2014) Sedimentation in the floodplains
479 of the Mekong Delta, Vietnam Part II: deposition and erosion, *Hydrol Processes* 28 (7), 3145-3160. doi:
480 <https://doi.org/10.1002/hyp.9855>.

481 Hung, N. N., Quan, L. Q. & Thanh, N. C. (2020) Impacts of riverbed lowering on tidal regimes in the Mekong Delta
482 river system and proposals for management solutions (in Vietnamese), *Vietnam J Hydrometeorol*, 715 (7),
483 59–67. doi: [https://doi.org/10.36335/vnjhm.2020\(715\).59-67](https://doi.org/10.36335/vnjhm.2020(715).59-67).

484 Jordan, C., Tiede, J., Lojek, O., Visscher, J., Apel, H., Nguyen, H. Q., Quang, C. N. X. & Schlurmann, T. (2019) Sand
485 mining in the Mekong Delta revisited-current scales of local sediment deficits, *Sci Rep*, 9 (1), 1-14. doi:
486 <https://doi.org/10.1038/s41598-019-53804-z>.

487 Kim, T. T., Huong, N. T. M., Huy, N. D. Q., Tai, P. A., Hong, S., Quan, T. M., Bay, N. T., Jeong, W.-K. & Phung, N.
488 K. (2020) Assessment of the impact of sand mining on bottom morphology in the Mekong River in an Giang
489 Province, Vietnam, using a hydro-morphological model with GPU computing, *Water*; 12 (10), 2912. doi:
490 <https://doi.org/10.3390/w12102912>.

491 Koehnken, L., Rintoul, M. S., Goichot, M., Tickner, D., Loftus, A. C. & Acreman, M. C. (2020) Impacts of riverine
492 sand mining on freshwater ecosystems: A review of the scientific evidence and guidance for future research,
493 *River Res Appl*, 36 (3), 362-370. doi: <https://doi.org/10.1002/rra.3586>.

494 Kondolf, G. M. (1997) PROFILE: Hungry water: effects of dams and gravel mining on river channels, *Environ*
495 *Manage*, 21 (4), 533-551. doi: <https://doi.org/10.1007/s002679900048>.

496 Kumm, M., Lu, X., Rasphone, A., Sarkkula, J. & Koponen, J. (2008) Riverbank changes along the Mekong River:
497 Remote sensing detection in the Vientiane–Nong Khai area, *Quat Int*, 186 (1), 100-112. doi:
498 <https://doi.org/10.1016/j.quaint.2007.10.015>.

499 Loc, H. H., Binh, D. V., Park, E., Shrestha, S., Dung, T. D., Son, V. H., Truc, N. H. T., Mai, N. P. & Seijger, C. (2021)
500 Intensifying saline water intrusion and drought in the Mekong Delta: From physical evidence to policy
501 outlooks, *Sci Total Environ*, 757, 143919. doi: <https://doi.org/10.1016/j.scitotenv.2020.143919>.

502 Luo, X.-L., Zeng, E. Y., Ji, R. Y. & Wang, C. P. (2007) Effects of in-channel sand excavation on the hydrology of the
503 Pearl River Delta, China, *J Hydrol*, 343 (3-4), 230-239. doi: <https://doi.org/10.1016/j.jhydrol.2007.06.019>.

504 Minderhoud, P. S. J., Coumou, L., Erkens, G., Middelkoop, H. & Stouthamer, E. (2019) Digital elevation model of
505 the Vietnamese Mekong delta based on elevation points from a national topographical map, *PANGAEA*. doi:
506 <https://doi.org/10.1594/PANGAEA.902136>.

507 Miyazawa, N., Sunada, K. & Sokhem, P. 2008 Bank erosion in the Mekong River Basin: Is bank erosion in my town
508 caused by the activities of my neighbours? *A Critical Review of Water and Development Concepts, Principles*
509 *and Policies*. Helsinki University of Technology: Helsinki, Finland: Water & Development Publications.

510 Moriasi, D. N., Gitau, M. W., Pai, N. & Daggupati, P. (2015) Hydrologic and water quality models: Performance
511 measures and evaluation criteria, *Trans ASABE*, 58 (6), 1763-1785. doi:
512 <https://doi.org/10.13031/trans.58.10715>.

513 Ng, W. X. & Park, E. (2021) Shrinking Tonlé Sap and the recent intensification of sand mining in the Cambodian
514 Mekong River, *Sci Total Environ*, 777, 146180. doi: <https://doi.org/10.1016/j.scitotenv.2021.146180>.

515 Padmalal, D. & Maya, K. 2014a Impacts of River Sand Mining. In: Padmalal, D. & Maya, K. (eds.) *Sand Mining:*
516 *Environmental Impacts and Selected Case Studies*. Dordrecht: Springer Netherlands.

517 Padmalal, D. & Maya, K. 2014b *Sand mining: environmental impacts and selected case studies*, Springer.

518 Park, E., Loc, H. H., Binh, D. V. & Kantoush, S. (2022) The worst 2020 saline water intrusion disaster of the past
519 century in the Mekong Delta: Impacts, causes, and management implications, *Ambio*, 51 (3), 691-699. doi:
520 <https://doi.org/10.1007/s13280-021-01577-z>.

521 Rentier, E. & Cammeraat, L. (2022) The environmental impacts of river sand mining, *Sci Total Environ*, 838, 155877.
522 doi: <https://doi.org/10.1016/j.scitotenv.2022.155877>.

523 Sonak, S., Pangam, P., Sonak, M. & Mayekar, D. 2006 Impact of sand mining on local ecology. *Multiple dimensions
524 of global environmental change*. Teri Press, New Delhi.

525 Thanh, V. Q., Reyns, J., Wackerman, C., Eidam, E. F. & Roelvink, D. (2017) Modelling suspended sediment dynamics
526 on the subaqueous delta of the Mekong River, *Cont Shelf Res*, 147, 213-230. doi:
527 <https://doi.org/10.1016/j.csr.2017.07.013>.

528 Van Rijn, L. C. 1993 *Principles of sediment transport in rivers, estuaries and coastal seas*, The Netherlands, Aqua
529 Publications: Amsterdam.

530 Vu, M. T., Luu, C., Bui, D. Q., Vu, Q. H. & Pham, M. Q. (2024) Simulation of hydrodynamic changes and salinity
531 intrusion in the lower Vietnamese Mekong Delta under climate change-induced sea level rise and upstream
532 river discharge, *Regional Studies in Marine Science*, 78, 103749. doi:
533 <https://doi.org/10.1016/j.rsma.2024.103749>.

534 Vu, T. H., Backhaus, L., Van Binh, D., Kantoush, S. A. & Stamm, J. (2025) Applying deep learning for boat detection
535 and numerical modeling to assess sand mining impacts on river morphology: A case study in the Vietnamese
536 Mekong Delta, *Geomorphology*, 490, 110010. doi: <https://doi.org/10.1016/j.geomorph.2025.110010>.

537 Winemiller, K. O., McIntyre, P. B., Castello, L., Fluet-Chouinard, E., Giarrizzo, T., Nam, S., Baird, I. G., Darwall, W.,
538 Lujan, N. K. & Harrison, I. (2016) Balancing hydropower and biodiversity in the Amazon, Congo, and
539 Mekong, *Science*, 351 (6269), 128-129. doi: <https://doi.org/10.1126/science.aac7082>.